Technical report: Partial wave analysis of the $\pi^0\pi^0\eta'$ Dalitz plot

Stefan Resag

Institut für Strahlen– und Kernphysik, Universität Bonn, D–53115 Bonn, Germany

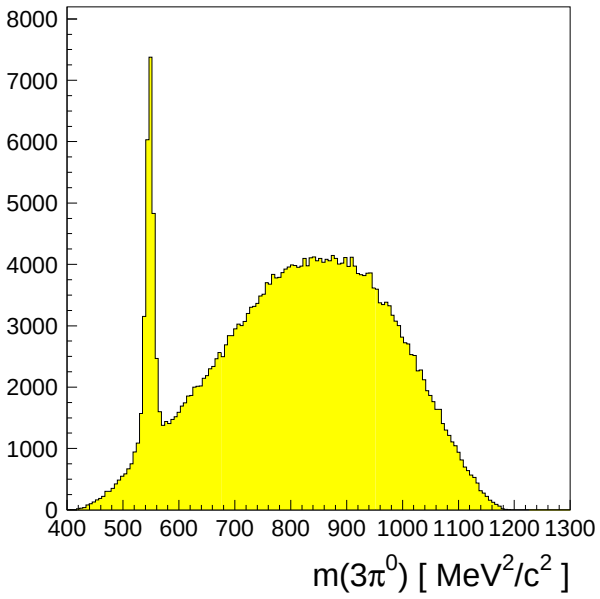

Figure 1:
The invariant $3\pi^0$ mass distribution of the $4\pi^0\eta$ final state (four entries/event).

1 The $4\pi^0\eta$ final state

Besides the $5\pi^0$ final state the $4\pi^0\eta$ final state is the only non-negligible contribution to the 10γ channel. The $4\pi^0\eta$ data offer some interesting aspects. The main selection criteria and cuts can be found in [1]. Similar to the $5\pi^0$ final state we distinguish between two different kinds of selections. Type I allows for one or more good kinematic fits for the hypothesis $\bar{p}p\rightarrow 4\pi^0\eta$ whereas type II allows only for exactly one good fit to this hypothesis. If the selction of the data set contains a cut on an invariant mass distribution then type I is the more appropriate type of selection since most of the combinatorical background is removed by the mass cut. A further reduction as done in type II would result in a reduction of the data signal.

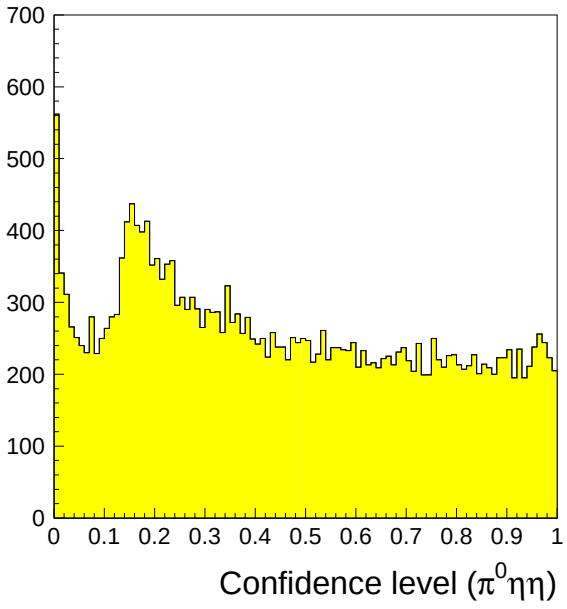

Figure 2:
Confidence level distribution of the kinematic fit $\bar{p}p\rightarrow\pi^0\eta\eta$. The depletion of events for $CL(\bar{p}p\rightarrow\pi^0\eta\eta) < 10\%$ is due to the cut on $Cl(\bar{p}p\rightarrow 4\pi^0\eta) \geq 10\%$.

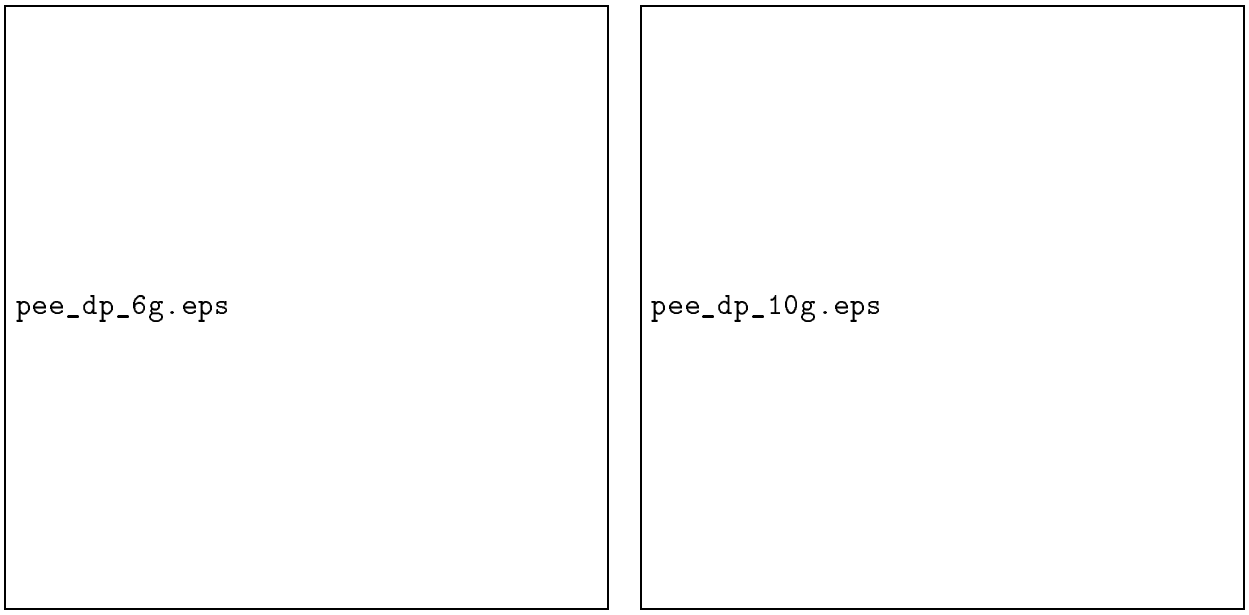

Figure 3: *The $\pi^0\eta\eta$ Dalitz plot for für $\bar{p}p\to 6\gamma$ (a)) and $\bar{p}p\to 10\gamma$ (b))*

1.1 The $\pi^0\eta\eta$ final state

The first selection type is used for generating events $\pi^0\eta\eta$. In Fig. 1 the $3\pi^0$ mass distribution for selection type I is shown. A clear η signal is observed with a background of about 20%. The events in the peak belong to the process $\bar{p}p\to\pi^0\eta\eta$. Events with a $3\pi^0$ mass in the range of 523 MeV to 575 MeV are kinematically fitted to the hypothesis $\bar{p}p\to\pi^0\eta\eta$ (10C-fit). The confidence level distribution (Fig. 2) shows a dip at low confidence levels due to the cut on $Cl(\bar{p}p\to 4\pi^0\eta) > 10\%$ done before. However for a further reduction of background the additional cut $Cl(\bar{p}p\to\pi^0\eta\eta) \geq 10\%$ is applied.

The resulting Dalitz plot (Fig. 3 b)) shows the same structures as the corresponding plot from 6γ data (Fig. 3 a)). This data have been selected and analysed in a work by R. Hackmann [2,3]. The crossed $a_0(980)$ bands and a structure at 1500 MeV, the $f_0(1500)$, are clearly visible. A blob at an invariant $\eta\eta$ mass of 1300–1400 MeV could be due to an $f_0(1370)$.

To demonstrate the compatibility of both data sets a constant background of 5% is subtracted from the $\pi^0\eta\eta$ Dalitz plot of the 10γ data sample similar to [2]. To take into account the further background of about 20% under the η signal (Fig. 1) Monte Carlo events of the type $\bar{p}p\to 4\pi^0\eta$ which are reconstructed in the $\pi^0\eta\eta$ Dalitz plot are subtracted from the data. However a significant deviation of both data set especially at higher $\pi^0\eta$ masses is observed (Fig. 5 a)). To remove these deviations the background of the process $\bar{p}p\to\pi^0\pi^0\eta'$ ($\eta'\to\pi^0\pi^0\eta$) has to be taken into account. These events reconstructed in the $\pi^0\eta\eta$ Dalitz plot cause a contribution deviating strongly from phase space. After subtraction of these events both data sets are in good agreement (Fig. 5 b) and c)). The combinatorical background doesn't play a significant role since we have only four entries per event in contrast to the $\pi^0\pi^0\eta$ Dalitz plot ($\bar{p}p\to\pi^0\pi^0\eta\to 5\pi^0$), were we have 10 entries per event in the $3\pi^0$ mass distribution.

For a better comparison of the 6γ and 10γ data sets the 6γ data are rebinned and both Dalitz plots are subtracted from each other taking the background into account. The resulting

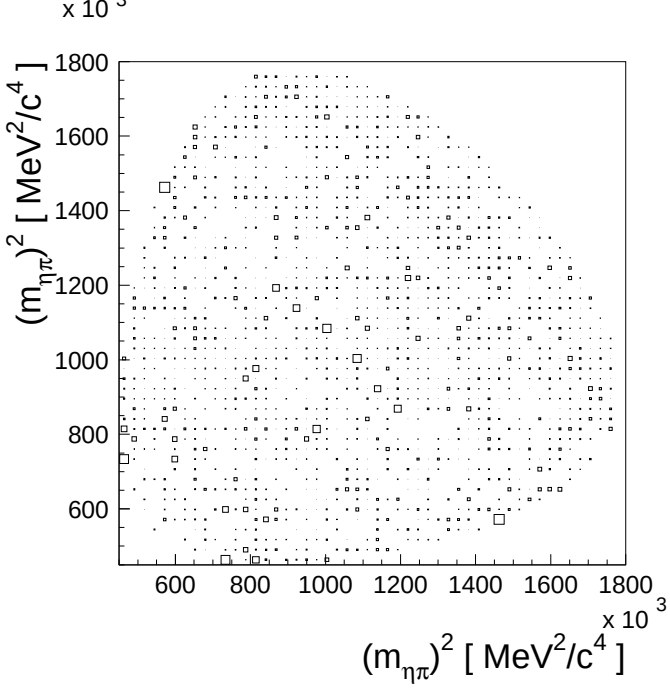

Figure 4:
The χ^2 distribution of the difference of the $\pi^0\eta\eta$ Dalitz plot of the 6γ and 10γ data set.

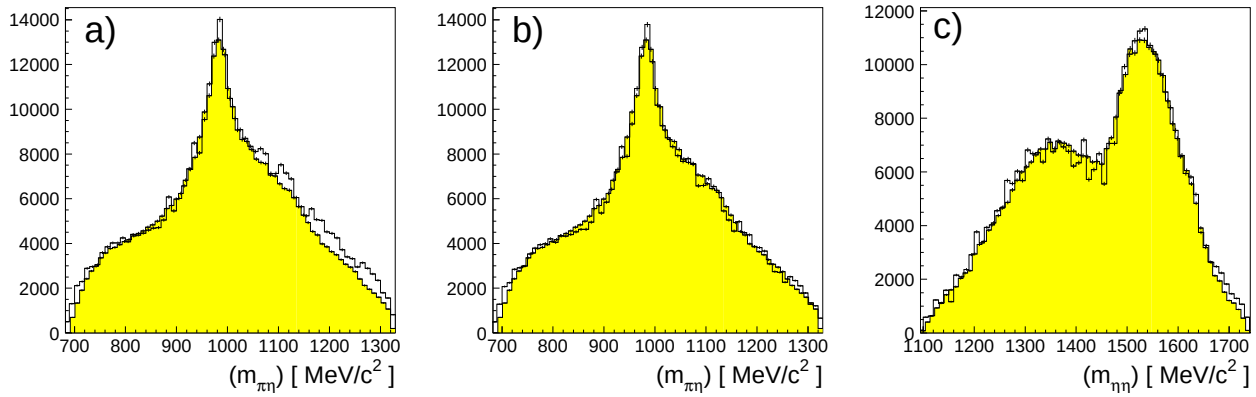

Figure 5: *The $m_{\pi\eta}$ und $m_{\eta\eta}$ distribution of the process $\bar{p}p\rightarrow\pi^0\eta\eta$. Grey: 6γ final state. White: 10γ final state. a) Without reduction of the $\pi^0\pi^0\eta'$ background. b) + c) After reduction of the $\pi^0\pi^0\eta'$ background.*

χ^2 per degree of freedom is 1.30. No significant deviation are found (see Fig. 4). Therefore both data sets are in good agreement and the selection is properly working for the $4\pi^0\eta$ channel. This also means that data sets containing a non-negligible background contribution can be understood.

2 The $\pi^0\pi^0\eta'$ Dalitz plot

The invariant $2\pi^0\eta$ mass distribution (see Fig. 6) of the $4\pi^0\eta$ final state shows two interesting structures. First of all a clear η' signal is visible corresponding to events of the type $\bar{p}p\rightarrow 2\pi^0\eta'$ ($\eta'\rightarrow\pi^0\pi^0\eta$). The signal is seated on a background contributing with about 40% to the whole signal. This background can be suppressed somewhat by removing events $\pi^0\eta\eta$ (grey histogram

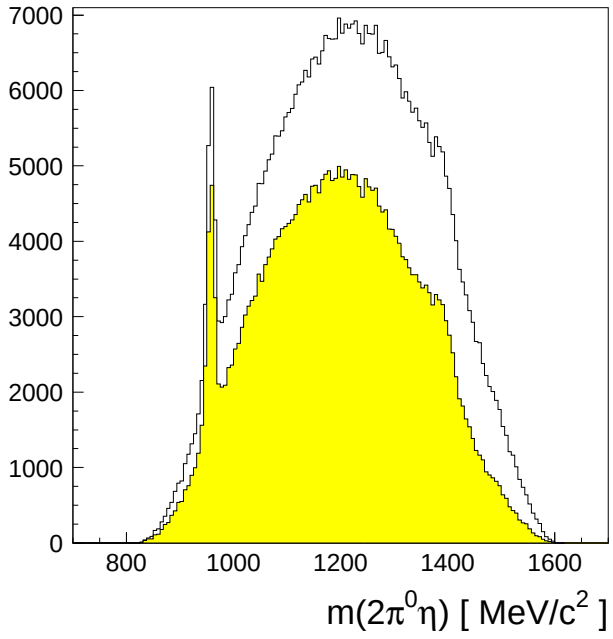

Figure 6:
The $2\pi^0\eta$ mass distribution before (white) and after (grey) the cut on events $\bar{p}p \to \pi^0\eta\eta$.

of Fig. 6). The second structure appears at a mass of about 1400 MeV. A similar structure has been observed in our $\pi^+\pi^-\pi^0\pi^0\eta$ data both in the $\pi^0\pi^0\eta$ and in the $\eta\pi^+\pi^-$ mass distribution. This shoulder is partly due to reflections of the η' signal. Furthermore the signal is generated by the E/ι meson with $I(J^{PC}) = 0(0^{-+})$ [4].

2.1 Background

The main interest of this report lies in the clear η' signal sitting on a large background. The description of the background is based on the assumption that the background under the signal causes the same distribution in the Dalitz plot as events lying in the so called 'side-bins'. With 'side-bins' we mean the regions in the invariant $\pi\pi\eta$ distribution below and above the resonance. To shift the side-bin events into the kinematic borders of the Dalitz plot they are kinematically fitted. We use for the two side-bins a mass range of (927MeV − 939MeV) and (975MeV − 987MeV), for the η' signal a mass window of (945MeV − 969MeV). This means that we have the same amount of events in the two side-bins and under the η' signal, because the background is more or less linear in the η' region. Before kinematic fitting of side-bin events energy and momentum are multiplied by a factor so that the invariant $\pi^0\pi^0\eta$ mass is exactly the η' mass.

The confidence level distribution of the hypothesis $\bar{p}p \to \pi^0\pi^0\eta'$ for data and Monte Carlo events is flat for events from the signal region. The side-bins show a decreasing distribution to higher confidence levels due to the wrong kinematics (see Fig. 7). From the left side-bin 27% and from the right side-bin 16% of the events are rejected by the kinematic fit. These regions therefore have to be scaled by a factor of 1.37 or 1.19, respectively, to achieve the correct amount of background events.

The Dalitz plot generated by subtraction of signal (Fig. 8 a)) and side-bin (Fig. 8 b) and c)) Dalitz plots should be free of background. Left and right background distribution look different; however the sum of both shows a structure at $m^2_{\eta'\pi^0_1} = 2.4 \cdot 10^6$ MeV^2, $m^2_{\eta'\pi^0_2} = 1.4 \cdot 10^6$ MeV^2

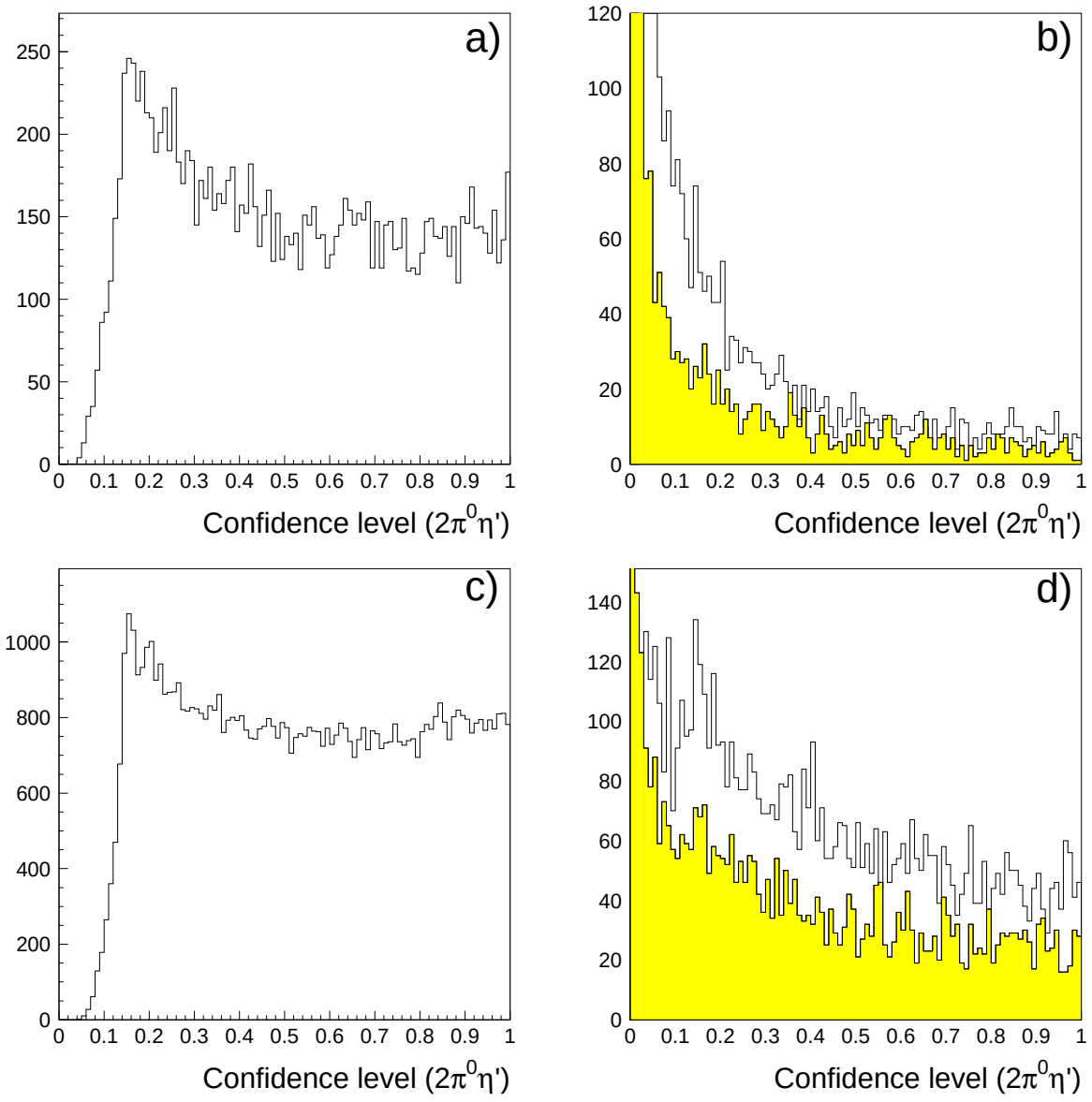

Figure 7: *Confidence level distribution of $\bar{p}p \to \pi^0\pi^0\eta'$. a) signal region. b) left (grey) and right (white) side-bin. c) and d): Same distributions for simulated events.*

that also appears in the data plot. Therefore it is plausible that the sum of both side-bins gives a good approximation to the real background distribution. In all other parts of the Dalitz plot were the data show significant structures the background is flat. Only 18% of the background can be asigned to combinatorical background. The main part is due to $4\pi^0\eta$ events being not generated through an intermediate η'. However phase space distributed $4\pi^0\eta$ events do not cause any significant structures in the $\pi^0\pi^0\eta'$ Dalitz plot (Fig. 9 a)). In contrast to that events reconstructed under the η' signal but belonging to wrong combinations $\pi^0\pi^0\eta$ of $\pi^0\pi^0\eta'$, $\eta' \to \pi^0\pi^0\eta$ cause a structure in the Dalitz plot similar to the background (Fig. 9 b)). The differences are probably due to dynamical processes in the $4\pi^0\eta$ channel, interferences and detector acceptance.

For estimation of the detector acceptance Monte Carlo events of the hypothesis $\pi^0\pi^0\eta'$ are

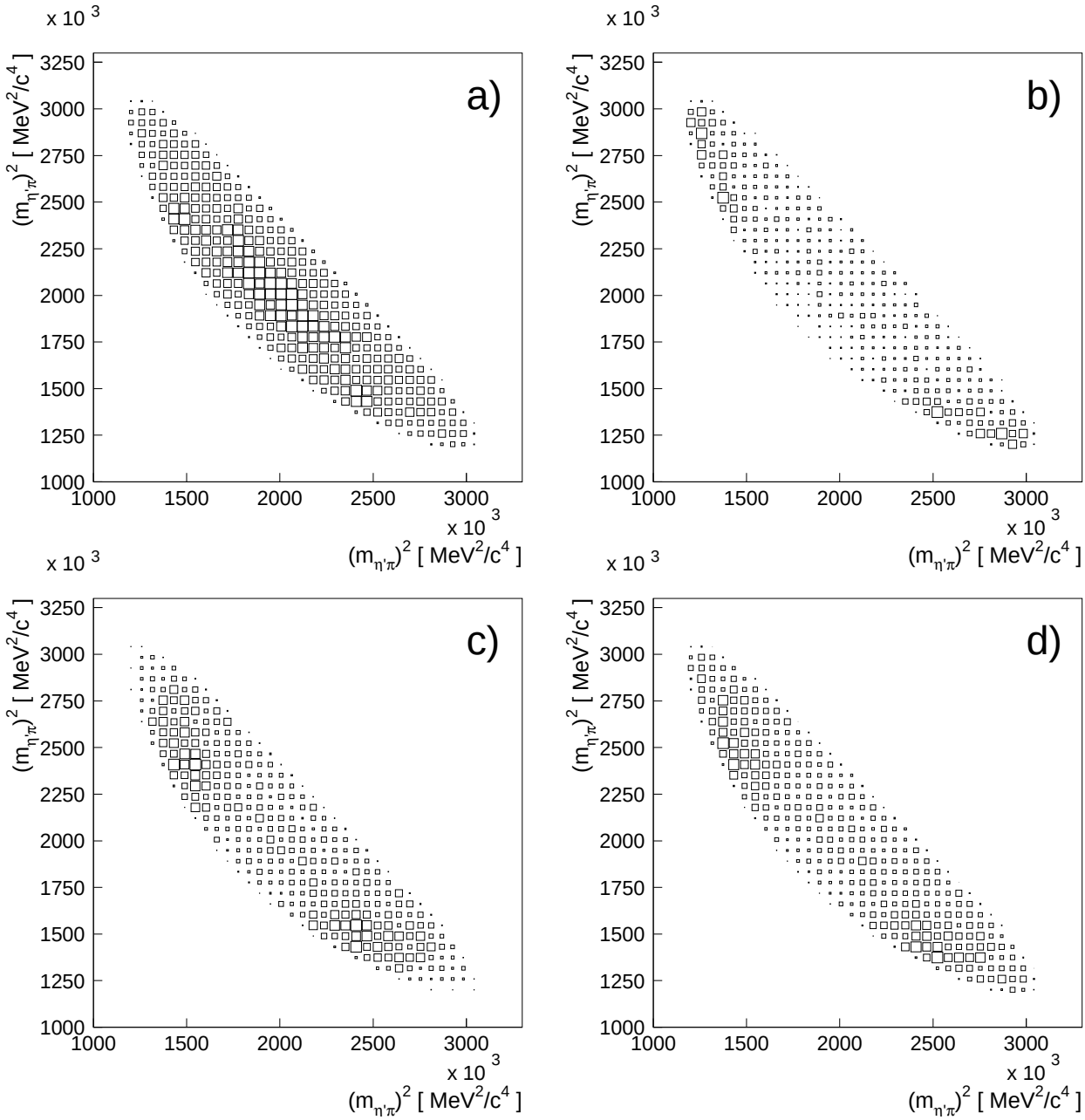

Figure 8: *The $\pi^0\pi^0\eta'$ Dalitz plot.* a) *$m_{2\pi^0\eta} \in$ (945 MeV, 969 MeV), b) $m_{2\pi^0\eta} \in$ (927 MeV, 939 MeV), c) $m_{2\pi^0\eta} \in$ (975 MeV, 987 MeV), d) Sum of b) and c).*

generated. The reduction of the background is done similar to the experimental data. The resulting acceptance corrected Dalitz plot is generated by dividing the data Dalitz plot by the Monte-Carlo Dalitz-plot neglecting bins with less than 5 events.

2.2 Partial wave analysis of the $\pi^0\pi^0\eta'$ Dalitz plot

The kinematically allowed region for the $\pi^0\pi^0$ system is limited to a range from 270 MeV to 957 MeV. In this region no coupling to the $\bar{K}K$ channel is allowed and therefore the $f_0(980)$

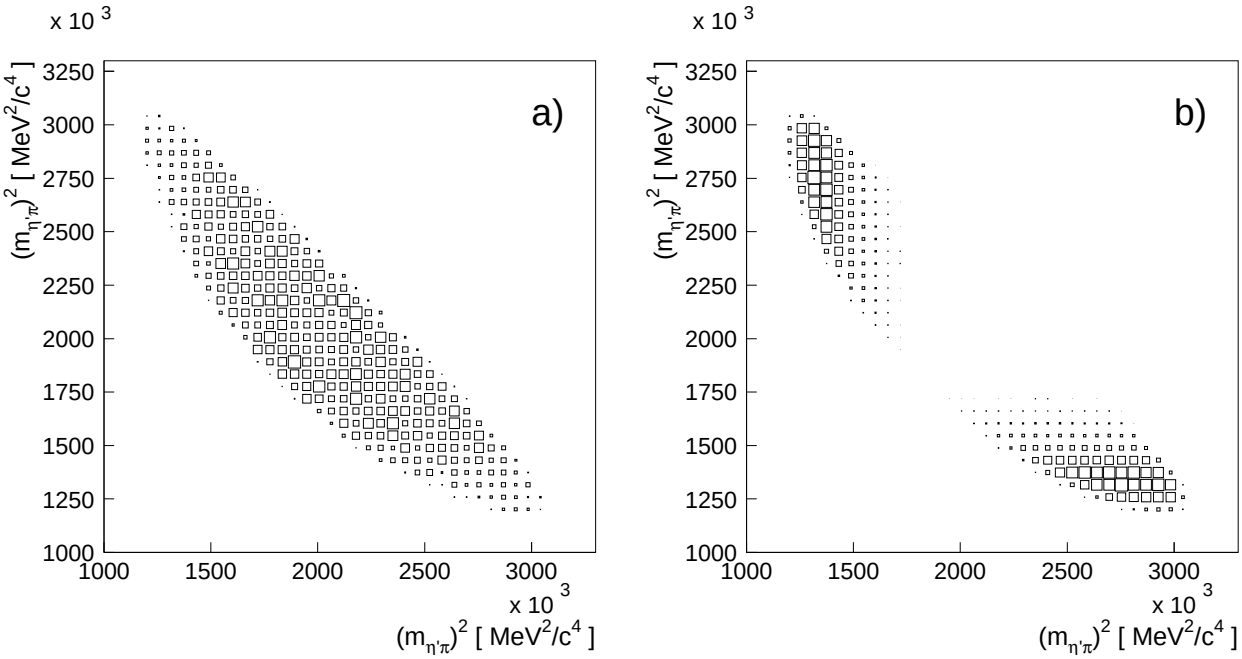

Figure 9: *Background distributions due to* a) *wrong combinations* $\eta' \to \pi^0\pi^0\eta$, b) $4\pi^0\eta$ *events (Monte Carlo).*

does not play any role in the description of the data. For relative angular momenta $l = 2$ the $f_2(1270)$ is dominant. Due to its high mass of 1270 MeV and a width of 185 MeV it can be neglected in the fits. For the $\pi\eta'$ interaction we have to take contributions in a mass range from 1090 MeV to 1740 MeV into account. Here the $a_2(1320)$, the $a_0(1450)$ and possibly the $a_2'(1650)$ from [5, 6] are possible resonances. The high energy tail of the $a_0(980)$ could in principle have effects on the $\pi\pi\eta'$ data set; however these should only be recognizable at much higher statistics. As mentioned above the smallest and most homogeneous background is in that region sensitive to the two resonances $a_2(1320)$ and $a_0(1450)$. To higher masses where the possible radial excitation $a_2'(1650)$ could lie less information is present since the background contribution and therefore the statistical errors are large. On the other hand this region will have little impact on the $a_2(1320)$ and the $a_0(1450)$. As a further contribution the π_1 with $I^G(J^{PC}) = 1^-(1^{-+})$ is considered. It has exotic quantum numbers and has been claimed by the GAMS collaboration as a resonant contribution in the reaction $\pi^- p \to \eta\pi^0 n$ [7]. In an analysis of of the $\pi^0\pi^0\eta$ final state by S. Spanier [8] a non-resonant behaviour was found; however the $\pi\eta$ P-wave (with quantum numbers of the π_1) contributed with 1.5–4.5% to the total final state depending on the model. Its mass and width could be varied in a range of 1200–1600 MeV and 400–1000 MeV, respectively, without significant changes in the quality of the fit. We consider both resonant and non-resonant behaviour of the $\pi\eta'$ P-wave.

The amplitudes for the fit of the $\pi^0\pi^0\eta'$ Dalitz plot are formulated using the K-matrix formalism in the P-vector approach [9, 10]. In case of the $\pi\eta$ S-, P- and D-wave were we have just one resonance in each partial wave, respectively, the amplitude reduces to a relativistic Breit-Wigner function. Solely the $\pi\pi$-S-wave is formulated as a 2×2-K-matrix using the parameters of [11]. Due to the limited statistics only annihilation from protonium state $^1S_0$ with $J^{PC} = 0^{-+}$ is taken into account.

The results of the partial wave analysis are summarized in Tab. 1. The data set is fitted in

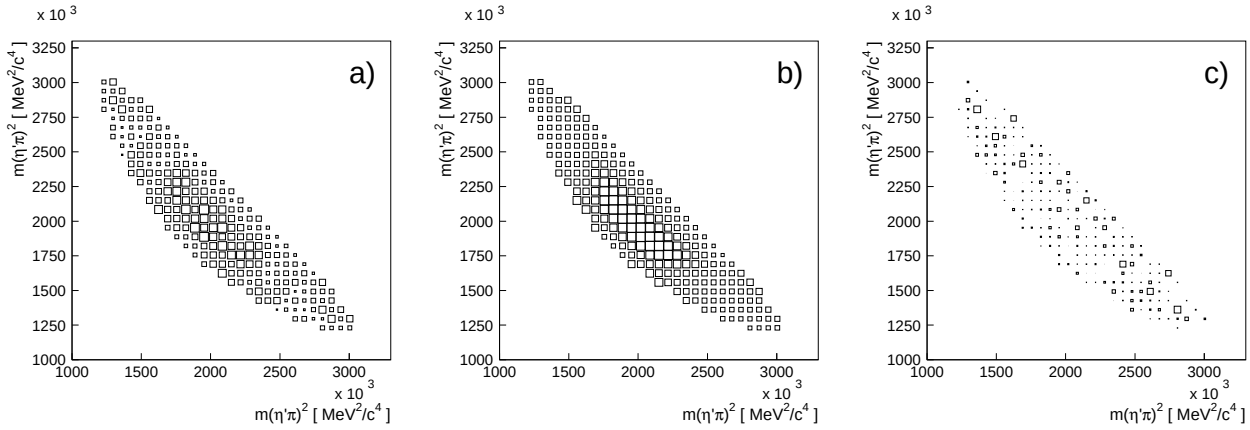

Figure 10: *Comparison of data and fit no. 4 of the $\pi^0\pi^0\eta'$ Dalitz plot. a) Background and acceptance corrected $\pi^0\pi^0\eta'$ Dalitz plot. b) $\pi^0\pi^0\eta'$ Dalitz plot due to fit no. 4. c) Corresponding χ^2 distribution from comparing data with fit no. 4.*

three different binnings of 30×30, 35×35 and 40×40 bins with 179, 246 and 311 bins, respectively, used in the fit. All other bins lie outside of phasespace or contain less than five entries. To study the effects of the background subtraction two different statistical errors are used for a Dalitz-plot bin. In the first method errors are calculated via Gaussian error propagation. In the second method the square root of the 'side-bin' entries after multiplication with the factors 1.19 and 1.37, respectively, are used as the statistical errors of the side-bin contributions. This causes an underestimation of the relative error of the side-bins by a factor of $1.09 = \sqrt{1.19}$ and $1.17 = \sqrt{1.37}$, respectively. The errors of the contributions of each resonance from Tab. 1 are calculated using the standard deviation of all fits to a certain hypothesis. The χ^2/ndf for both methods is calculated from the three binnings of the Dalitz plot. As a reference we use fit no. 4. All other χ^2 values together with the errors are calculated as follows:

$$\begin{aligned} \bar{\chi^2_j} &= \bar{\chi^2_4} + \frac{1}{3}\sum_{i=1}^{3}(\chi^2_{ij} - \chi^2_{i4}) \\ \sigma(\chi^2_j) &= \sqrt{\frac{1}{2}\left(\sum_{i=1}^{3}\left((\chi^2_{ij} - \chi^2_{i4}) - (\bar{\chi^2_j} - \bar{\chi^2_4})\right)^2\right)} \end{aligned} \tag{1}$$

The sum goes over the three different binnings. This method allows for valuation of the statistical significance of relative distances of χ^2 values.

We start with the hypothesis $\bar{\mathrm{p}}\mathrm{p} \to \eta'(\pi\pi)_S$, were $(\pi\pi)_S$ are two pions in relative S-wave (no. 1). A satisfactory discription of the data is not given ($\chi^2/ndf \approx 1.90$). The respective addition of an $a_0(1450)$ or an $a_2(1320)$ (no. 2 u. 3) with fixed parameters gives a large improvement in χ^2. We find a further significant improvement when imposing both resonances at the same time (no. 4). The data are described very accurately. A comparison of the background and acceptance corrected Dalitz plot with fit no. 4 and the corresponding χ^2 distribution is given in Fig. 10.

The influence of the $a_0(1450)$ on the quality of the fit can be seen in the $\pi^0\eta'$ mass distribution. In Fig. 11 a comparison of this distribution is shown for fits no. 3 and 4. Without

No.	1	2	3	4	5	6	7	8
$(\pi\pi)_S$								
%	100	88.7 ± 3.1	96.9 ± 0.6	93.8 ± 0.4	93.7 ± 1.0	94.4 ± 1.0	53.4 ± 5.6	87.0 ± 5.0
$a_0(1450)$								
m [MeV]	–	1450	1450	1450	1450	1450	1650 ± 60	1450
Γ [MeV]	–	260	–	260	260	260	730 ± 70	260
%	–	11.3 ± 3.1	–	4.1 ± 0.8	3.5 ± 0.9	2.0 ± 1.6	46.2 ± 5.5	4.7 ± 1.5
$a_2(1320)$								
m [MeV]	–	–	1320	1320	1320	1360 ± 20	1320	1320
Γ [MeV]	–	–	110	110	110	160 ± 40	110	110
%	–	–	3.1 ± 0.6	2.1 ± 0.5	1.6 ± 0.5	3.6 ± 0.6	0.4 ± 0.1	1.7 ± 0.6
π_1								
m [MeV]	–	–	–	–	1405	–	–	1530 ± 70
Γ [MeV]	–	–	–	–	180	–	–	440 ± 100
%	–	–	–	–	1.2 ± 0.6	–	–	6.6 ± 4.0
χ^2/ndf								
Meth. 1	1.87 ± 0.23	1.20 ± 0.02	1.12 ± 0.06	0.98	0.97 ± 0.1	0.93 ± 0.02	0.94 ± 0.01	0.96 ± 0.1
Meth. 2	2.01 ± 0.25	1.30 ± 0.04	1.21 ± 0.10	1.05	1.04 ± 0.01	1.01 ± 0.01	1.02 ± 0.01	1.03 ± 0.01

Table 1: *Results of the parial wave analysis of the* $\pi^0\pi^0\eta'$ *Dalitz plot.*

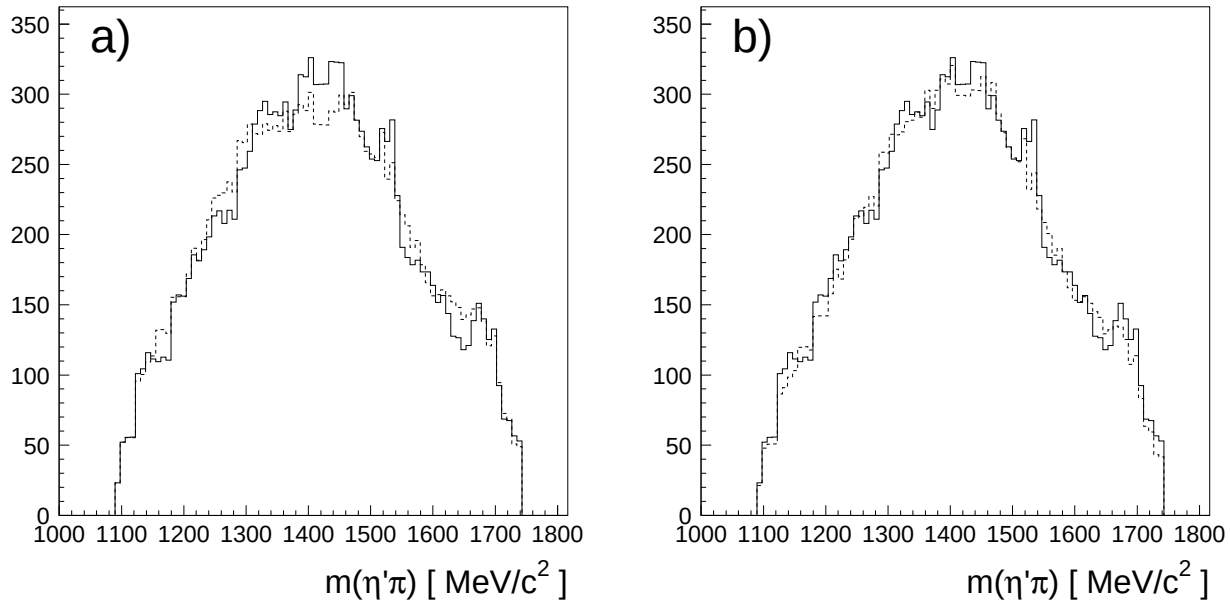

Figure 11: *Comparison of data and fits. a) without $a_0(1450)$, b) with $a_0(1450)$*

the $a_0(1450)$ we find deviations in the center and the sides of the distribution (Fig. 11 b)). These disappear when adding the $a_0(1450)$ (Fig. 11 b)). No further systematic deviations are ovserved.

Adding the π_1 causes a slight improvement in the absolute χ^2 value; however the value for χ^2/ndf remains the same due to additional fit parameters. The influence of this resonance on the other contributions exept of $(\pi\pi)$-S-wave is small. Introducing the π_1 with fixed mass and width from [7] (no. 5) it contributes with 1.2% to the whole data set. Using instead free mass and width its contribution increases to $(6.6 \pm 4.0)\%$ with a mass of m = 1500 MeV (no. 8). It becomes very broad ($\Gamma \approx 440$ MeV) so that possibly parts of the $\eta'\sigma$ contribution are described by the π_1.

In fits no. 6 and 7 mass and width of the $a_2(1320)$ and the $a_0(1450)$, respectively, are left free. For the $a_2(1320)$ we find $m = 1360 \pm 20$ MeV und $\Gamma = 160 \pm 40$ MeV. These values are compatible with [12] due to the large error bars. Finding values for the $a_0(1450)$ of $m = 1650 \pm 60$ MeV and $\Gamma = 730 \pm 70$ MeV the data are not sensitive to mass and width of the $a_0(1450)$.

To test the significance of single contributions a series of fits has been done. If the $a_0(1450)$ is substituted by a constant contribution χ^2/ndf deteriorates to the value of fit no. 3. The most significant feature of the data is the $a_2(1320)$. It is not possible to get a good fit without a tensor contribution. The data aren't to sensitive to the detailed shape of the $\pi\pi$-S-wave. Using different parametrisations from other analyses do not cause any variation. Even using a constant amplitude for the $\pi\pi$-S-wave gives a χ^2/ndf lying between that of fit no. 3 and 4.

Next the influences of the resonance parameters on the contributions to the $\pi^0\pi^0\eta'$ final state are considered. The values for $a_2(1320)$ are known very accurately ($m = 1318.4 \pm 0.6$ MeV, $\Gamma = 107 \pm 5$ MeV). Varying them in the range of errors doesn't have any effects.

The values for the $a_0(1450)$ are much less accurately known. In [8] the parameters are

No.	$m_{a_0(1450)}$	$\Gamma_{a_0(1450)}$	Contrib. $a_0(1450)$	Contrib. $a_2(1320)$
1	1450	230	3.0	2.0
2	1450	260	4.1	2.1
3	1450	300	6.8	2.1
4	1450	330	9.0	2.1
5	1420	260	2.9	2.2
6	1450	260	4.1	2.1
7 8	1520	260	6.0	1.6
9	1430	230	2.3	2.2
10	1500	300	8.6	1.6
11	1520	330	11.9	1.4

Table 2: *Effects of the values of mass and width of the* $a_0(1450)$ *on the* $a_2(1320)$ *and* $a_0(1450)$ *branching ratio based on hypothesis no.*

determined to $m = 1450 \pm 40$ MeV und $\Gamma = 270 \pm 40$ MeV. In [13] mass and width of 1470 ± 25 MeV and $\Gamma = 265 \pm 30$ MeV, respectively, are quoted. A variation of the parameters in these ranges has large effects on the $\bar{\mathrm{p}}\mathrm{p} \to a_0(1450)\pi^0$ ($a_0(1450) \to \eta'\pi^0$) branching ration. A survey is given in Tab. 2.

The $a_2(1320)$ contribution is very stable under variation of $\Gamma_{a_0(1450)}$ whereas the $a_0(1450)$ contribution becomes larger with increasing width. Raising $m_{a_0(1450)}$ the $a_2(1320)$ contribution decreases significantly. Refering to the values of the coupled channel analysis [13] the branching ratio of the $a_2(1320)$ based on hypotheses no. 3, 4, 5, and 8 is given by

$$\frac{Br(\bar{\mathrm{p}}\mathrm{p} \to a_2(1320)\pi^0)}{Br(\bar{\mathrm{p}}\mathrm{p} \to \pi^0\pi^0\eta')} = (2.1 \pm 0.5 \pm 0.5 \pm 0.3)\% = (2.1 \pm 0.7)\%. \quad (2)$$

The first and second error is due to statistical and systematical error taken from Tab. 1; the third error is due to variations of the $a_0(1450)$ parameters. Since we expect the three errors to be independent of each others the are added quadratically. The hypotheses no. 6 and 7 are not considered for determination of branching ratios, since the resonance values are badly determined.

The $a_0(1450)$ branching ratio shows much stronger variations. This is mostly due to the less significant structures of S-wave resonances. Therefore parts of the $\pi\pi$-S-wave could be described by the $a_0(1450)$ (see also Tab. 1 fits no. 2 and no. 7). Furthermore an incorrect description of the background could be compensated by a larger contribution of the $a_0(1450)$. A cautious estimate using hypotheses no. 4, 5 and 8 gives

$$\frac{Br(\bar{\mathrm{p}}\mathrm{p} \to a_0(1450)\pi^0)}{Br(\bar{\mathrm{p}}\mathrm{p} \to \pi^0\pi^0\eta')} = \left(3.9 \pm 0.9 \pm 0.6^{+3.0}_{-1.5}\right)\% = \left(3.9^{+3.2}_{-1.5}\right)\%. \quad (3)$$

The meaning of the errors is similar to eq. 2.

For estimation of the branching ratio $Br(\bar{\mathrm{p}}\mathrm{p} \to \pi^0\pi^0\eta')$ Monte Carlo events of the type

$\bar{p}p \to \pi^0\pi^0\eta'$ are produced and are undertaken the identical selection chain as real data. The Monte Carlo errors are scaled to achieve flat confidence level distributions and Gaussian pulls.

Starting with 14534000 experimental data without charged tracks we find 8230 events $\bar{p}p \to \pi^0\pi^0\eta'$. Starting with 685000 Monte Carlo events without charged tracks 62300 are reconstructed in the η' signal. With $Br(\pi^0 \to \gamma\gamma) = 0.988$, $Br(\eta \to \gamma\gamma) = 0.388$, $Br(\eta' \to \pi^0\pi^0\eta) = 0.208$ and 4.0% all neutral events from $\bar{p}p$ annihilation at rest in liquid hydrogen we find

$$Br(\bar{p}p \to \pi^0\pi^0\eta') = (3.2 \pm 0.3) \cdot 10^{-3}. \tag{4}$$

The error is dominated by systematic effects and is estimated to 10%.

The absolute branching ratios of $a_2(1320)$ and $a_0(1450)$ can now be calculated:

$$Br(\bar{p}p \to a_2(1320)\pi^0 \to \pi^0\pi^0\eta') = (6.7 \pm 2.8) \cdot 10^{-5} \tag{5}$$

$$Br(\bar{p}p \to a_0(1450)\pi^0 \to \pi^0\pi^0\eta') = (12.5^{+10.4}_{-5.2}) \cdot 10^{-5}. \tag{6}$$

For comparison of the $a_2(1320)$ branching ratio with other experiments we use the ratio of branching ratios of the $\eta'\pi^0$ and $\eta\pi^0$ decay. The latter has been determined in [13] to $(2.05 \pm 0.40) \cdot 10^{-3}$). We find

$$R(a_2(1320)) = \frac{Br(a_2(1320) \to \eta'\pi)}{Br(a_2(1320) \to \eta\pi)} = 0.033 \pm 0.015. \tag{7}$$

This is in good agreement with two measurements of the VES collaboration [14, 15] who find a ratio of $R = 0.040 \pm 0.007$. Neglecting hypotheses no. 5 and 7 (the π_1 is not considered) this ratio can be altered to 0.033 ± 0.010.

For the $a_0(1450)$ we find

$$R(a_0(1450)) = \frac{Br(a_0(1450) \to \eta'\pi)}{Br(a_0(1450) \to \eta\pi)} = 0.43^{+0.39}_{-0.24}. \tag{8}$$

The branching ratio $Br(\bar{p}p \to a_0(1450)\pi^0 \to \pi^0\pi^0\eta) = (0.29 \pm 0.11) \cdot 10^{-3}$ is taken from [13].

The branching ratios can be compared to predictions of $SU(3)_{flavor}$. As a consequence of the quark-line rule (OZI-rule) couplings to $\bar{s}s$ components of the η or η' are neglected. The coupling therefore occours only via the $(\bar{u}u + \bar{d}d)$ component of the wave functions. This means for the ratio of branching ratios [16]

$$R = \frac{F_L^2(q_{\pi^0\eta'})}{F_L^2(q_{\pi^0\eta})} \cdot \frac{q_{\pi^0\eta'}}{q_{\pi^0\eta}} \cdot \tan^2(90^\circ - \Theta_{id} + \Theta_{PS}), \tag{9}$$

with a pseudoscalar mixing angle Θ_{PS} of $(-17.3 \pm 1.8)^\circ$ from [16] and an ideal mixing angle Θ_{id} of 35.3°. The decay momenta $q_{\pi^0\eta'}$ and $q_{\pi^0\eta}$ correspond to the phase space factors. The function $F_L^2(q)$ describes the angular momentum barrier in the decay of a resonace with relative angular momentul L between the decay particles. For $L = 0$ $F_L^2(q)$ is just a constant. This results in a ratio of

$$R(a_0(1450)) = 0.38 \pm 0.06, \tag{10}$$

being in good agreement with our result (eq. 8). The errors of $R(a_0(1450))$, however, could be reduced by a better knowledge of the $a_0(1450)$ parameters.

For the determination of the $a_2(1320)$ ratio we need an ansatz for $F_L^2(q)$. The best known is $F_L^2(q) = q^{2L}$ [17] and is an approximation for small values of q. This ansatz starts from point like particles

$$R(a_2(1320)) \quad = \quad 0.027 \pm 0.004. \tag{11}$$

For extendet particles we use a Blatt-Weiskopf parametrisation [18]. For a relative angular momentum of two it is given by

$$F_L^2(q) \quad = \quad \frac{(qr)^4}{\left((qr)^2 - 3\right)^2 + 9(qr)^2}. \tag{12}$$

The mean range parameter r of the decay potential is depending strongly on the size of the mesons and should lie in a range of 0.2 fm to 1.0 fm. We find

$$R = 0.12 \text{ for } r = 1.0 \text{ fm} \tag{13}$$

and

$$R < 0.048 \text{ for } r < 0.54 \text{ fm} \; . \tag{14}$$

The latter value gives an upper limit for our value of R. In investigations of decays of tensor mesons a value of (0.20 ± 0.04) fm for r is determined [19] in good agreement with our result.

Finally we conclude that the branching ratios determined above are in good agreement with $\mathrm{SU}(3)_{flavor}$. The introduction of a mean range of the decay potential with a maximum value of 0.5 fm is supported by our result. A value of 0.8 – 1.2 fm proposed by [20] is in contradiction to our result. The existence of the exotic π_1 can neither be extracted nore is it excluded by our data.

3 Further data of the $4\pi^0\eta$ final state

We now want to discuss the remaining mass distributions of the $4\pi^0\eta$ final state. As mentioned above it is convenient to use selection type II (exactly one good fit to the 9C hypothesis) for data not selected including a cut on a special mass distribution in the selection chain. All other cuts follow the selection of the $5\pi^0$ final state. As for $5\pi^0$ data a significant reduction of combinatorical background and $5\pi^0$ background is expected. A detailled investigation of the background is beyond this work and therefore not performed.

The confidence level distribution shows a flat behaviour after reduction of the $5\pi^0$ background (Fig. 12) and is similar to that of simulated events.

The $2\pi^0$ mass distribution (Fig. 13) does not show any significant structures. A clear $a_0(980)$ is observed in the $\eta\pi^0$ mass distribution. The $3\pi^0\eta$ distrubion only differs slightly from phase space whereas the $4\pi^0$ spectrum shows a significant enhancement at the upper limit of phase space. This indicates strong $4\pi^0$ dynamics at higher masses and could be due to the $f_0(1500)$. Because of limited phase space ($M_{4\pi^0} < 1330$ MeV) the information on $4\pi^0$ resonances is reduced in comparison to $5\pi^0$ data.

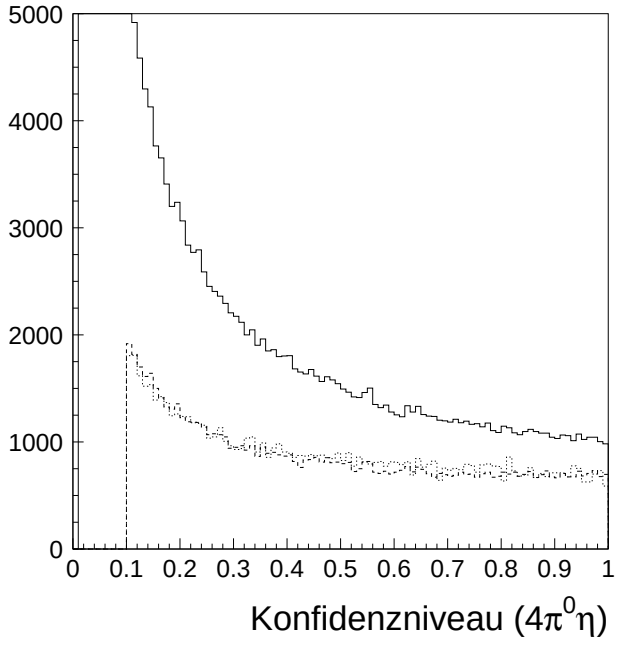

Figure 12:
Confidence level distribution of the kinematic fit to $4\pi^0\eta$. Solid: The best confidence level from the kinematic fit for each event. Dashed: after all cuts. Dotted: Monte Carlo Events.

References

[1] A. Abele et al., Phys. Lett. **B380** (1996) 453.

[2] R. Hackmann, Dissertation, Universität Mainz (1994)

[3] C. Amsler et al., Phys. Lett. **B353** (1995) 571

[4] C. Amsler et al., Phys. Lett. **B358** (1995) 389

[5] S. Spanier, Dissertation, Universität Mainz (1994)

[6] J. Lüdemann, Dissertation, Universität Bochum (1995)

[7] M. Boutemeur, M. Poulet, Hadron '89, ed. F. Binon, J.M. Frère, J.P. Peigneux - (Ed. Frontières 1989) 119

[8] C. Amsler et al., Phys. Lett. **B333** (1994) 277

[9] I. Aitchison, Nucl. Phys. **A189** (1972) 417

[10] S.U. Chung et al., Ann. Phys. **4** (1995) 404

[11] C. Amsler et al., Phys. Lett. **B342** (1995) 433

[12] Review of Particle Physics, Phys. Rev. **D54** (1996) 1

[13] C. Amsler et al., Phys. Lett. **B355** (1995) 425

[14] G.M. Beladidze et al., Z. Phys. **C54** (1992) 235

[15] G.M. Beladidze et al., Phys. Lett. **B313** (1993) 276

[16] C. Amsler et al., Phys. Lett. **B294** (1992) 451

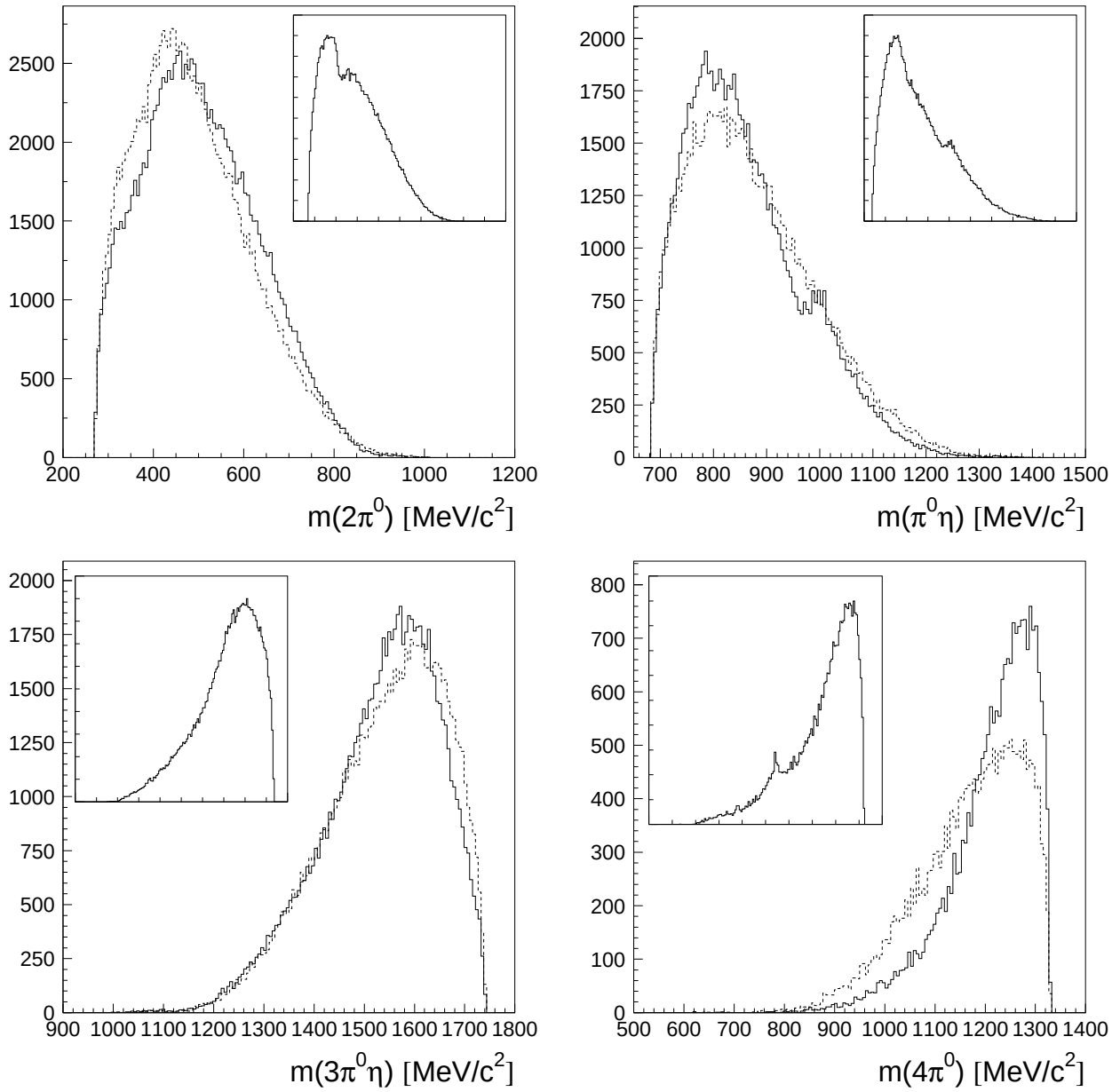

Figure 13: *Invariant mass distributions of the $4\pi^0\eta$ final state. Small histograms: without subtraction of the $\pi^0\eta\eta$ and $\pi^0\pi^0\eta'$ final state. Large histograms: data (solid) and Monte Carlo events (dashed) after subtraction of the $\pi^0\eta\eta$ and $\pi^0\pi^0\eta'$ signals. The $3\pi^0$ and $2\pi^0\eta$ mass distribution of this data set is shown in Fig. 1 and 6.*

[17] C.B. Dover, P.M. Fishbane, Nucl. Phys. **B244** (1984) 349

[18] F. V. Hippel, C. Quigg, Phys. Rev. **5** (1972) 624

[19] K. Peters, E. Klempt, Phys. Lett. **B352** (1995) 467

[20] C.B. Dover, P.M. Fishbane, S. Furui, Phys. Rev. Lett. **57** (1986) 1538